Towards Accurate Unsteady Real-Time Helicopter Aeroacoustic Analysis Using GPU-CUDA Accelerated Tools

Acoustics Session

Luís Cruz
Aeroacoustics Engineer
CEIIA, Aerodynamics Dept
luis.cruz@ceiia.com

Alessandro Scandroglio
Senior Aerodynamics Specialist
AgustaWestland, Aerodynamics Dept.
alessandro.scandroglio@agustawestland.com

Abstract

With the constant pursuit for more fuel efficient and less noisy helicopters, there is a requirement for numerical tools capable of faster aerodynamic and acoustic analysis. This work describes the development of a new aeroacoustic framework that takes advantage of the CUDA (Compute Unified Device Architecture) framework, speeding up calculations by more than 2 orders of magnitude when compared with single thread CPU versions. The implemented framework is shown in detail and two different studies are presented to highlight the different capabilities. The first case study involves an unsteady analysis of an isolated MR (Main Rotor) where the speed and accuracy requirements are balanced, but mainly focused on maximizing the calculation speed. For the second case study a fully unsteady analysis of a coupled MR and TR (Tail Rotor) is performed to show the capability of the framework to carry out complex analysis in relatively short computational times.

1 Introduction

The distinctive noise of a helicopter is often considered a source of great annoyance. This is especially true in the approach phase where the tonal components, in the form of BVI (Blade Vortex Interaction), dominate the noise spectrum. Given that the helicopter is close to the ground and near or above populated areas, the perceived noise will be high and for more sensitive areas limitations can be imposed on helicopter operations. It is then important to minimize the rotor noise, either by using rotor technologies (passive or active) or by using landing procedures that minimize the on-ground noise by avoiding the Blade Vortex Interaction region.

In order to avoid excessive computational time when doing helicopter rotor aeroacoustic analysis, compromises must often be done. Simpler aerodynamic models or assume quasi-steady manoeuvres mean faster analysis but the unsteady effects which significantly affect BVI noise are missed. By taking advantage of the computational power made available by the use of GPUs (Graphic Processor Units) through the CUDA framework we are able to carry out very fast free-wake aerodynamic and acoustic analysis that can be used to optimize any flight path of any helicopter rotor configuration in close to real-time speed.

2 Literature Review

The work of Ikaida *et al*[1][2] focused on developing a real-time trajectory optimization based on numerical simulations. Since the noise source model had to be simple enough to allow real-time calculations, noise data obtained from flight experiments was reduced to simple equations. These equations had a modified flight path angle that took into consideration the effect of accelerating/decelerating helicopter, as this has a very big effect on the occurrence of BVI.

A more advanced procedure was developed by Brentner *et al*[3] where a complex 80 second manoeuvre was analysed by the loosely coupled GENHEL–PSU-WOPWOP system. GENHEL, a flight simulator code, implements a blade element

representation of the rotor, a three state Pitt-Peters dynamic inflow model and rigid motion of the blades is included. GENHEL was used to both perform the flight mechanics and provide the aerodynamic loading for the acoustic tool PSU-WOPWOP. PSU-WOPWOP is based on Farassat's Formulation 1A and implements the source-time dominant integration due to its superior efficiency for analysing unsteady manoeuvres. A very coarse azimuth step of 15.5 deg and 10 radial stations per blade were used to simulate both the aerodynamics and the acoustics resulting in a 4x slower than real-time simulations.

A similar work done by Hennes *et al*[4] and also Chen[5], studied unsteady flight manoeuvres using a 'time-accurate free-vortex rotor wake model and a manoeuvring rotor noise prediction code' and it was found that both the magnitude and directivity is significantly affected by BVI interactions which depend on the unsteady rotor wake development. The acoustic code used is also PSU-WOPWOP. The unsteady aerodynamics coupled a Weissinger-L lifting-surface model with a free-wake model and an azimuth step of 2.5deg was used and it is mentioned that a 10s manoeuvre "usually takes days to accomplish the job"[5].

Another approach is to use a quasi-steady approach[6][7][8] with an acoustic database (in the form of noise hemispheres) to be pre-calculated (either numerically or experimentally). Although the acoustic simulation of flight paths is very quick, the creation of the acoustic database can take several days (numerically) or require a lot of flight testing (experimentally). Additionally, if the database is numerically calculated, the unsteady effects of transient manoeuvres are only approximated or neglected altogether. This requires the flight paths to be smooth trajectories with small accelerations.

To dramatically speed up the aerodynamic tool calculations, M. Syal *et al*[9] applied the Fast Multipole Method (FMM) to reduce the computational complexity of very large simulations and also use the computational horsepower of GPUs using the CUDA framework. They demonstrated that a single GPU direct implementation (without FMM) was around 1000 times faster than a single thread CPU direct implementation. The GPU+FMM implementation was only found to be useful for very large analysis. For smaller analysis, similar to the ones being studied here, the GPU direct implementation is superior as the overhead associated with the FMM calculations is not compensated by the lower computational complexity.

Each of the works presented above has some limitation, be it the simplified models or the very slow computational speed. Our work combines the accuracy provided by the unsteady free-wake methods with the speed offered by the GPU implementation using the CUDA framework.

3 Parallel Processing using CUDA

CUDA was introduced in November 2006 and its new programming model and architecture take advantage of the GPU inherently parallel compute engine to solve computational problems in shorter times compared to a CPU. CUDA allows programmers to develop application software that easily scales its parallelism so that it fully uses GPUs with varying number of cores. The demand for real-time, high definition 3D graphics has pushed the GPU to evolve into a highly parallel, multithreaded, many-core processor with teraflop compute capability. A comparison between the evolution of GPU/CPU computational horsepower and memory bandwidth is presented below.

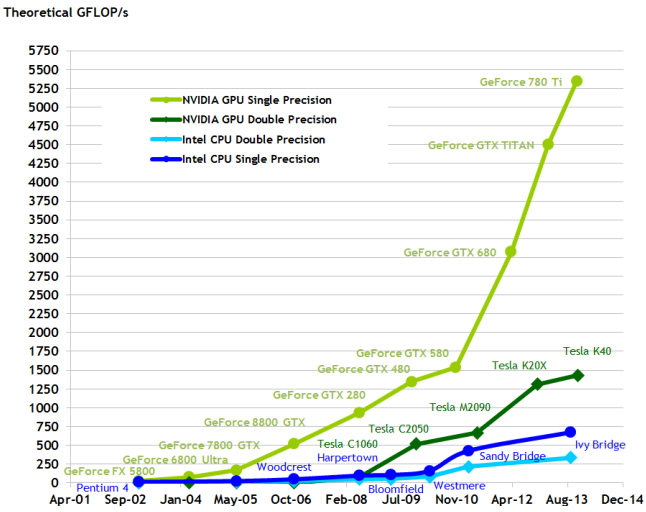

Figure 1 - Comparison between GPU and CPU processing power[10]

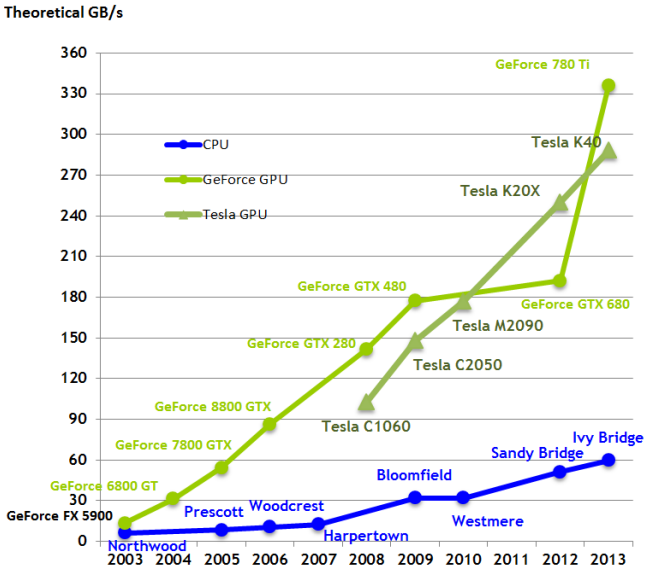

Figure 2 - Comparison between GPU and CPU memory bandwidth[10]

GPUs are especially well-suited to problems with data-parallel computations and high arithmetic intensity. This is the case of the Unsteady Free Wake Vortex Lattice Method where the wakes' self-induced velocity calculations require billions of independent Biot-Savart kernel evaluations per second. The source-time acoustic formulation implemented using CUDA is again well suited to be parallelized in a way that fully utilizes the computational power offered by GPUs.

4 Implemented Aeroacoustics Framework

Our current implementation framework is detailed in Figure 3. The flight path is provided by an optimizer and includes the spatial location and speed of the helicopter (4D trajectory). This flight path is analysed by a helicopter flight mechanics tool capable of determining the required controls to follow the desired trajectory. If the trajectory is deemed flyable, the controls time-history is passed on to the aeroacoustic framework where the aerodynamic tool will calculate the aerodynamic loading that the acoustic tool requires to calculate the noise on the desired locations. The ultimate goal for real-time acoustic analysis will require both the aerodynamic and acoustic tool to be working in parallel, but the current implementation has them working independently.

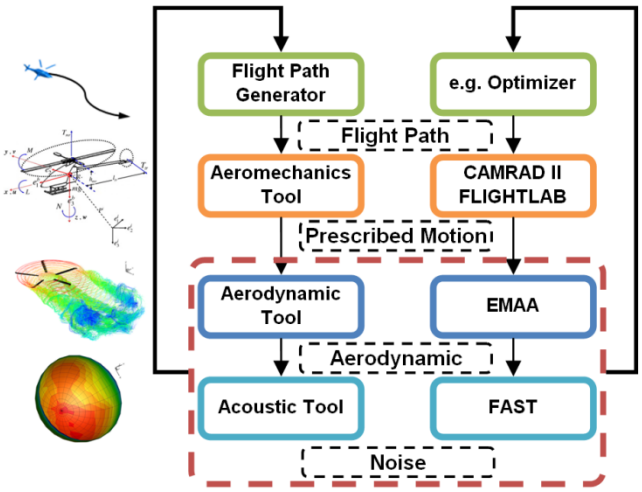

Figure 3 - Implemented aeroacoustics framework

4.1 Aerodynamic Analysis Tool

A new aerodynamic solver tool named EMAA (Enhanced Multi-GPU Aerodynamic Analysis) was developed inside AgustaWestland to exploit the computational power of multi-GPU and multi-CPU hardware.

4.1.1 Theory

EMAA's framework is based on the Vortex Lattice Method (VLM) so the lifting surfaces are assumed to be thin (i.e. with no thickness). Since the boundary conditions are enforced in the actual lifting surface, it can have camber and various planform shapes. If the flow is considered to be incompressible and irrotational it is governed by the simplified continuity equation given by

(1) $$\nabla^2 \Phi = 0$$

For a submerged body in the fluid, the velocity component must be tangent to the lifting surface and to the other solid boundaries, and in a body-fixed coordinate system

(2) $$\nabla \Phi \cdot \vec{n} = 0$$

In the above equation $\vec{n}$ is a vector normal to the body's surface, Φ is the velocity potential and $\vec{V} = \nabla \Phi$. The physical problem of finding the velocity field for the flow created is now reduced to the problem of solving the Laplace's equation for the

velocity potential with suitable boundary conditions. In VLM the lifting surfaces are divided into panels and to each panel a vortex ring is attached. The boundary condition that must be satisfied by the solution is the zero normal flow across the thin wing's solid surface given by

(3) $$\nabla(\Phi+\Phi_\infty)\cdot\vec{n}=0$$

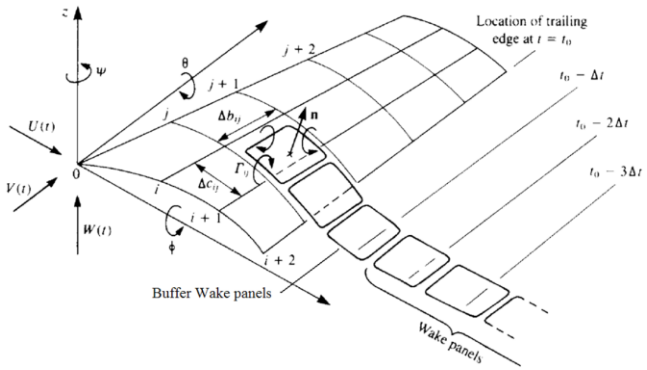

Figure 4 - Vortex Ring Model for a thin lifting surface[11]

Along the wing trailing edges, the trailing vortex of the last panel row must be cancelled to satisfy the three-dimensional trailing edge Kutta condition. This is done by attaching a row of vortex rings that cancel the vorticity as can be seen in the figure below. This row is also known as Buffer Wake.

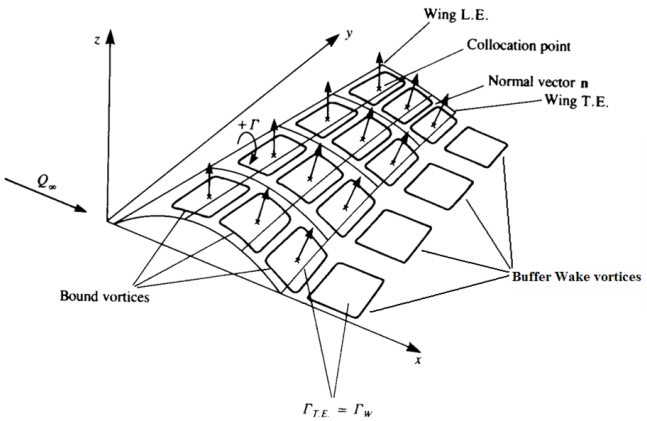

Figure 5 - Vortex ring model for a thin lifting surface[11]

The way one finds the velocity induced by a vortex segment/filament in a collocation point is by applying the Biot-Savart law.

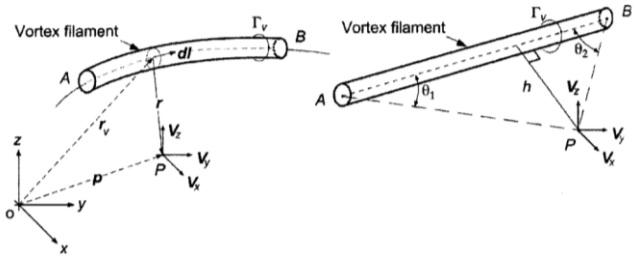

Figure 6 - Evaluation of the induced velocity from a vortex filament using the Biot-Savart law. Left - Curved vortex. Right - Straight-line vortex[12]

The incremental values of the induced velocity $d\vec{v}$ on a point P at a distance $\vec{r}$ from the vortex segment $d\vec{l}$ with strength Γ_v can be written in general form as

(4) $$d\vec{v}=\frac{\Gamma_v}{4\pi}\frac{d\vec{l}}{|\vec{r}|^3}$$

The total velocity at point P is then obtained by integration along the lengths of the vortex filament and given by

(5) $$\vec{V}_p=\frac{\Gamma_v}{4\pi h}(\cos\theta_1-\cos\theta_2)\cdot\vec{e}$$

Since the Biot-Savart law is singular when $h=0$ it is necessary to use a finite core model. In this work the Vatistas swirl velocity model with $n=2$ is used to avoid the singularity and as a result the velocity induced by a straight segment is given by

(6) $$\vec{V}=\frac{\Gamma_v}{4\pi}\frac{h}{\left(r_c^4+h^4\right)^{1/2}}\left(\cos\theta_1-\cos\theta_2\right)\cdot\vec{e}$$

A viscous core growth model, based on the vortex age and vortex Reynolds number, is also used to account for the vortex strength dissipation due to viscous effects. This is given by

(7) $$r_c(t)=\sqrt{r_{c0}^2+4\alpha\delta\upsilon\, t}$$

where r_{c0} is the initial core radius, $\alpha=1.25643$, $\delta=1+a_1\,\mathrm{Re}_V$ is the eddy viscosity coefficient with $\mathrm{Re}_V=\Gamma_V/\upsilon$, υ is the air kinematic viscosity and a_1 is Squire's parameter and its value is determined from experimental measurements.

A hybrid free-wake method was implemented in EMAA as it combines the numerical stability offered by the VR (Vortex Ring) free-wake method used in the near-field and the computational efficiency of the CVC

(Constant Vorticity Contours) used in the far-field. The discreet concentrations of wake vorticity which characterize the CVC method can induce unrealistic blade pressure fluctuations and to avoid this phenomenon the transition from near-field to the far-field is moved away from the blade trailing edge. To further improve the computational speed and stability, a wake cut-off strategy is employed, with the older wake segments being removed from the free-wake calculations based on their age.

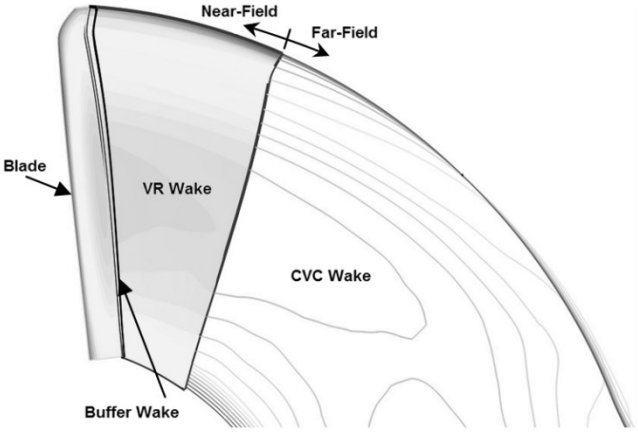

Figure 7 - Schematic showing the hybrid free-wake implemented in EMAA

For typical analysis, the most time consuming routine is the free-wake motion, where billions of Biot-Savart kernel evaluations must be performed every iteration. Particular attention was given to this routine in order to maximize the GPUs throughput by using the very fast on-chip Shared Memory and also the SFUs (Special Function Units) which are able to calculate complex mathematical functions by hardware rather than software. The final result was a GPU calculation speed of more than 1000x faster than on the CPU single core implementation.

4.1.2 Validation

The first set of results compares the C_L of different aspect ratio rectangular wings to the results obtained by Katz *et al*[11]. All the wings have the same chord of 0.5m and the span is varied from 2.0m (aspect ratio of 4.0) to 50000m (equivalent to aspect ratio of ∞). The velocity chosen was 10.0m/s and so the time-step calculated is 0.003125s as given by

(8) $$\Delta t = \frac{c}{16 \cdot U_\infty}$$

All the wings have the same angle of attack of 5° and are discretized using 4 chordwise panels and 13 spanwise. The results are presented below.

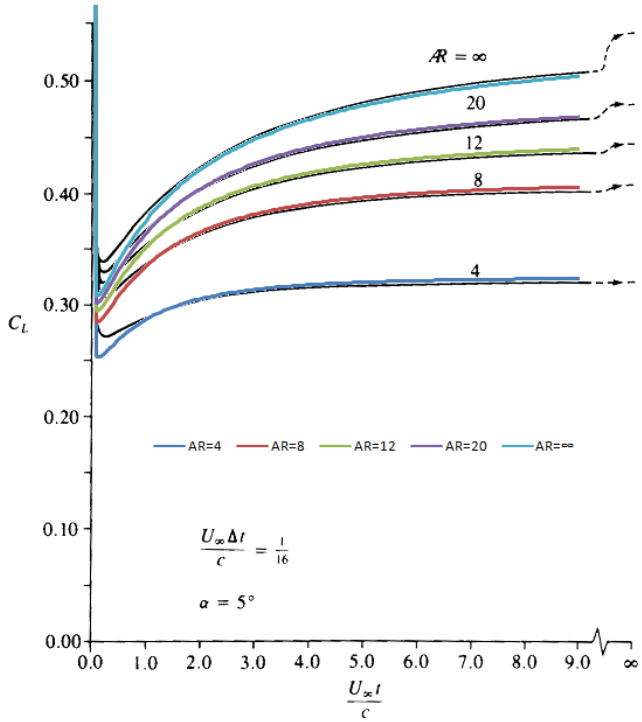

Figure 8 - Comparison of the results for the transient lift coefficient variation with time for uncambered, rectangular wings that were suddenly set into constant-speed flight. Colour lines represent the results of numerical solution (Adapted from Katz *et al*[11])

Another test to validate the computational implementation and in particular the unsteady load variation is to compare the numerical results with the analytical solution of Wagner, which is valid only for the two dimensional case or the same as the three dimensional case with infinite aspect ratio. This solution was obtained by Bisplingghoff *et al*[13] and gives the lift using equation

(9) $$L = \pi \cdot \rho \cdot U_\infty^2 \cdot c \cdot \alpha_0 \cdot \phi(s)$$

where

(10) $$\phi(s) = 1 - 0.165e^{-0.0455s} - 0.335e^{-0.3s}$$

with α_0 being the initial angle of attack and s the travelled distance in chord lengths.

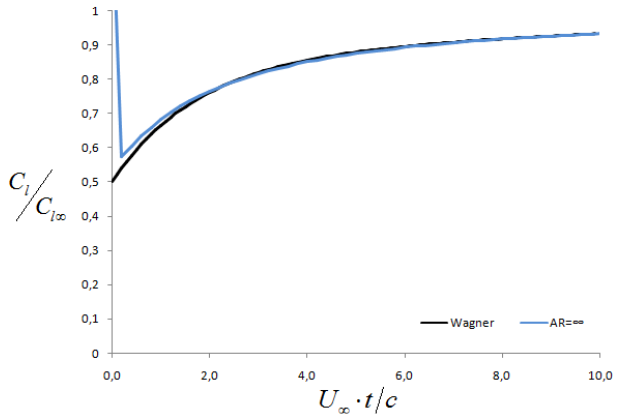

Figure 9 - Transient lift variation for an aerofoil suddenly set into motion. Comparison between the results of the Tool and the results from Wagner's analytical solution.

Further validation was performed against ADPANEL[14], another AW aerodynamic tool already extensively validated and used in helicopter design[15].

4.2 Acoustic Analysis Tool

In parallel to the development of EMAA, a new acoustic tool named FAST (Farassat-1A Acoustic Solver Tool) was also developed to exploit the same multi-GPU and multi-CPU hardware. The unsteady motion framework implemented in EMAA is also used in FAST to enable a seamless integration of both tools. The FAST tool implements the integral representation of the non-porous (and porous) FW-H equation known as Farassat's Formulation 1A[16] and using the source time dominant algorithm. This algorithm has several advantages compared to the observer-time dominant algorithm, the most significant one being the more straightforward parallelization. Additionally it was found to be numerically more efficient, especially for unsteady manoeuvres[17]. Since the aerodynamic loading is calculated by a Lifting Surface method, the compact chord approximation is used for the calculation of the Loading noise. This greatly speeds up the calculations without a significant impact on the calculated Loading noise[18].

4.2.1 Theory

In 1969 Ffowcs Williams and Hawkings[19] published their now classic paper which generalized Lighthill's acoustic analogy approach to include the effects of general types of surfaces and motions. The FW-H equation can be derived by extending the definition of fluid properties such that inside the moving surface the flow parameters have the same fluid state as the undisturbed medium. This extension is required because the wave equation needs to be valid in the entire three-dimensional space so that the simple Green's function of the wave equation in unbounded space can be used. An artificial discontinuity across all flow parameters will exist on the data surface (the blade's surface in the case of the non-porous formulation) which requires the use of generalized functions theory (or distributions theory) to deal with the derivatives of these flow parameters, which are present in the continuity and conservation of momentum equations. The derivation of the non-porous Formulation 1A is very well explained by Farassat[16] and its extension to a porous data surface was done by Di Frescantonio[20]. For completeness we merely present the final Thickness and Loading noise integral equations, valid for both porous and non-porous data surfaces. Defining the variables U_i and L_i as

$$U_i = \left(1 - \frac{\rho}{\rho_0}\right) v_i + \frac{\rho}{\rho_0} u_i \tag{11}$$

$$L_i = P_{ij} \cdot n_j + \rho u_i \left(u_n - v_n\right) \tag{12}$$

we have that the Thickness noise equation is

$$4\pi p'_T(\mathrm{x},t) = \int_{\tilde{f}=0} \left[\frac{\rho_0 U_n c\left(M_r - M_i^2\right)}{r^2 \left(1 - M_r\right)^3} \right]_{ret} dS + \int_{\tilde{f}=0} \left[\frac{\rho_0 \dot{U}_n}{r\left(1 - M_r\right)^2} + \frac{\rho_0 U_n \hat{r}_i \dot{M}_i}{r\left(1 - M_r\right)^3} \right]_{ret} dS \tag{13}$$

and the Loading noise equation is

$$4\pi p'_L(\mathrm{x},t) = \int_{\tilde{f}=0} \left[\frac{\dot{L}_i \hat{r}_i}{cr\left(1 - M_r\right)^2} + \frac{L_i \dot{M}_i \hat{r}_i^2}{cr\left(1 - M_r\right)^3} \right]_{ret} dS + \int_{\tilde{f}=0} \left[\frac{L_i \hat{r}_i - M_i L_i}{r^2 \left(1 - M_r\right)^2} + \frac{L_i \hat{r}_i \left(M_r - M_i^2\right)}{r^2 \left(1 - M_r\right)^3} \right]_{ret} dS \tag{14}$$

By considering the non-porous boundary conditions where $u_i = v_i$ and $\rho = \rho_0$, the non-porous equations derived by Farassat are recovered. Also, in the case of the porous formulation, the Thickness and Loading terms no longer represent Thickness and Loading noise as they do for the non-porous formulation because they now include the influence of the nonlinear sources around the blade.

4.2.2 Validation

The FAST tool was simply validated against already recognized AW internal tools[21], namely BENP and MARTA. The key advantages of FAST with respect to these tools are the faster calculation speed, easier setup and the straightforward integration with the EMAA tool.

5 Aeroacoustic Analysis

The application of the EMAA+FAST aeroacoustic chain will include an isolated MR analysis preceded by a study to understand the best configuration to maximize speed without a significant penalty to the accuracy. After that, a coupled MR and TR unsteady analysis will highlight the capabilities of EMAA+FAST to analyse very complex aeroacoustic cases.

5.1 Problem Setup

The helicopter model used in this work is a 6500kg machine equipped with articulated MR and TR as detailed by Melone *et al*[22]. The two rotors are oriented such as the MR is rotating counter-clockwise (when viewed from above) while the TR is rotating with the advancing side down (ASD), i.e., the TR thrust is pointing starboard. The TR is tilted at 15° of cantilever angle which allows the rotor to not only have a side force but also a vertical thrust component. A central center of gravity positioning has been assumed for the calculation of the helicopter trim states. The MR and TR blades have been assumed to be rigid in flap and pitch modes and have been equipped with AgustaWestland proprietary airfoils as well as the twist, chord and sweep distributions are taken from proprietary designs. The principal geometric and operating parameters for the MR and TR of the conceptual helicopter are summarized in Table 1 below.

	Main Rotor	Tail Rotor
Number of Blades	5	4
Rotor Radius	R	R_t=0.2R
Thrust weighted chord	0.064R	0.028R
Angular velocity	Ω	Ω_t=5Ω

Table 1 - Rotors Data

5.2 MR Steady Analysis

Before moving on to more complicated analysis, a study of different wake parameters, blade mesh and temporal resolution will be performed to highlight their impact on calculation speed and accuracy from which the best compromise will be chosen. This study will focus on a steady MR descent manoeuvre using the controls mentioned in the work of Melone *et al*[22] for Flight Condition 3 (FL3). The three certification microphone positions are used to compare the sound pressure of different meshes, wake refinements and azimuth step. The left microphone is placed 150m to the port side of the helicopter, the central microphone is below the helicopter path and the right microphone one is 150m on starboard side of the helicopter.

The baseline analysis (black lines) was done using a lifting surface with 30x30 panels (chordwise x spanwise) while the wake consisted of only vortex ring elements as our experience showed that it does not suffer from some of the problems of the CVC wake. The smallest azimuth step of 1.8° was chosen so that the maximum frequency was 40 times the Blade Passage Frequency (BPF) and this was found to be enough to capture the high frequency noise induced by BVI.

For the first set of results the azimuth step chosen was 1.8°. Figure 10 to Figure 12 compare the sound pressure using 2 different meshes, one with a 16x30 discretization (solid colour lines) and the other with a 8x25 discretization (dashed colour lines). The results difference between both meshes are very small apart when the courser wake is used. Three different CVC wake refinements were used, with CVC=1.0 (red lines) representing a refined wake, CVC=3.0 (blue lines) representing an intermediate wake refinement and CVC=5.0 (green lines) representing a course wake. It's clear that the wake refinement has a big impact on the BVI intensity with the CVC=5.0 wake having the biggest differences and the CVC=1.0 wake closely matching the baseline (incidentally, the free-wake

calculation time of the baseline and CVC=1.0 was almost the same). Given the more discreet nature of the CVC wake it is expected that the BVI interactions will be stronger when the wake refinement is coarser as the individual segments have more concentrated vorticity. This highlights that although potentially more efficient in terms of calculation speed, the CVC wake can be responsible for unrealistic BVI data.

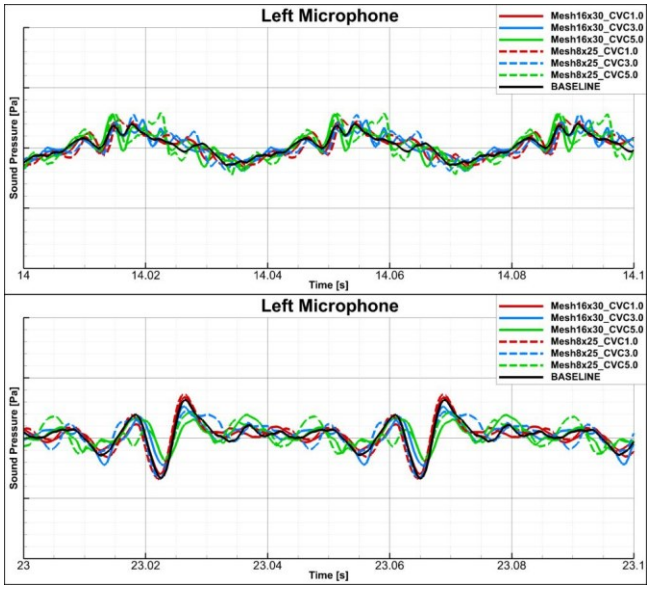

Figure 10 - Sound pressure on the left microphone for different meshes and CVC refinements and Δψ=1.8°

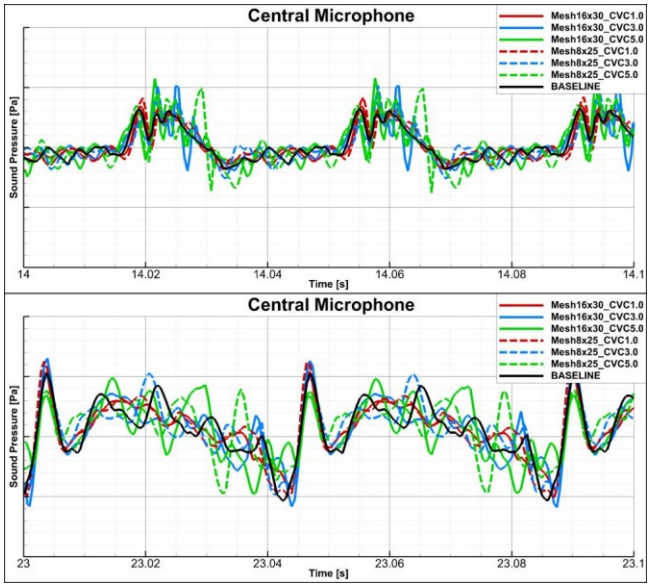

Figure 11 - Sound pressure on the central microphone for different meshes and CVC refinements and Δψ=1.8°

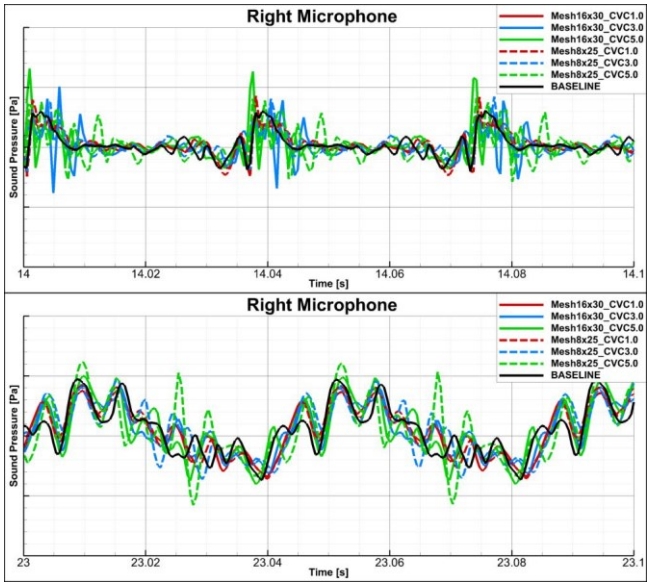

Figure 12 - Sound pressure on the right microphone for different meshes and CVC refinements and Δψ=1.8°

The results when the azimuth step is set to 2.8125° (maximum frequency of 25 times the BPF) are shown in Figure 13 to Figure 15. The CVC=1.0 wake case still closely matches the baseline case while the less refined wake cases are now closer to the baseline, in particular when CVC=3.0. By limiting the maximum frequency of the aerodynamic analysis, the unrealistically high BVI characteristic of the courser wakes is smoothed out.

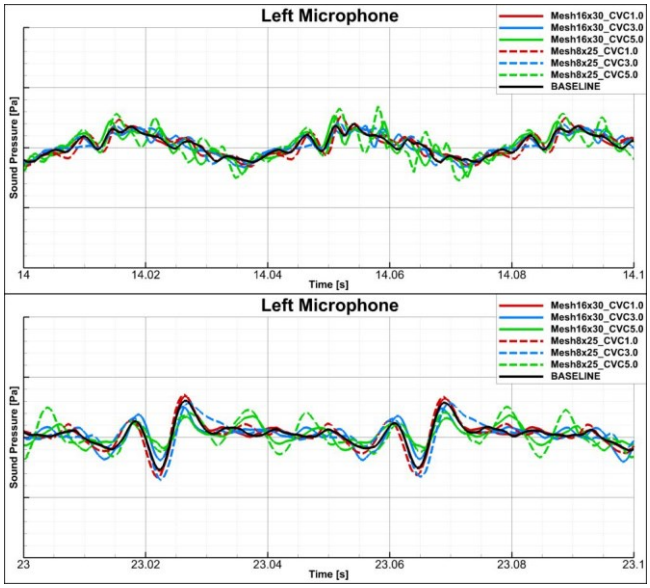

Figure 13 - Sound pressure on the left microphone for different meshes and CVC refinements and Δψ=2.8125°

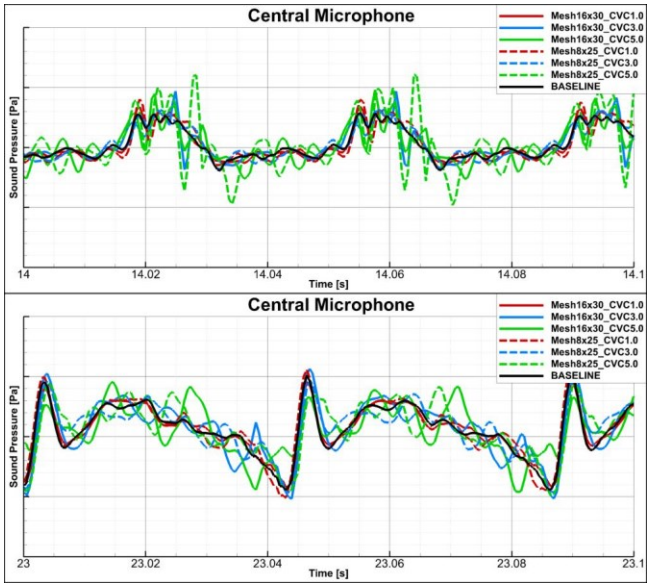

Figure 14 - Sound pressure on the central microphone for different meshes and CVC refinements and Δψ=2.8125°

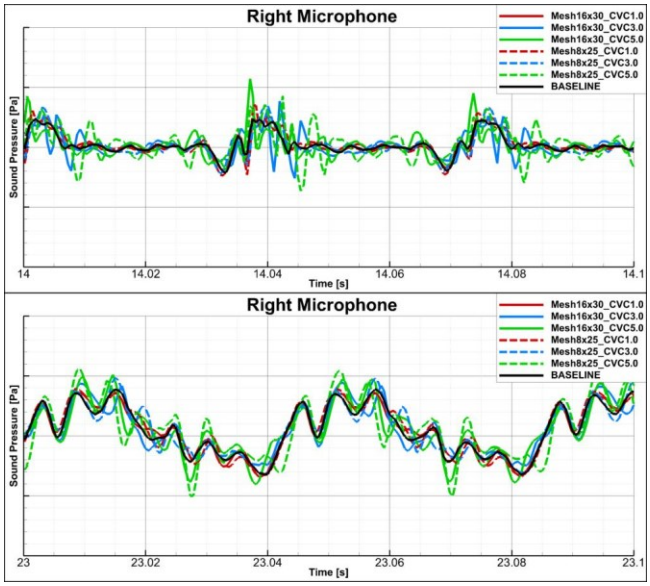

Figure 15 - Sound pressure on the right microphone for different meshes and CVC refinements and Δψ=2.8125°

The effect of different Δψ is clearly seen in Figure 16, where the A-Weighted Overall Sound Pressure Level (OASPL-dBA) along the descent path is compared for the same mesh and wake refinement but different Δψ. The general trend is that by increasing the Δψ, the OASPL-dBA will decrease as the higher frequency noise is missed and is in line with what is expected. The Δψ=2.8125° case is very similar to the other more refined cases, only missing out the baseline peak on the right microphone. The Δψ=2.8125°, CVC=3.0 and 8x25 mesh is close to 10 times faster than the baseline case and the differences are in general smaller than 5dBA for most of the path which is an acceptable compromise given the superior calculation speed. Less refined wakes and/or meshes do not provide considerable speed gains as the free-wake calculations are no longer the more time consuming part of the code and other overheads limit further speed increases. This is why this configuration was chosen for subsequent analysis.

Note that the OASPL-dB (no A-Weighting) comparison (not shown) revealed that the total acoustic energy is very similar for all the cases and that it should not be used to assess if a certain wake or mesh refinement is correctly capturing BVI.

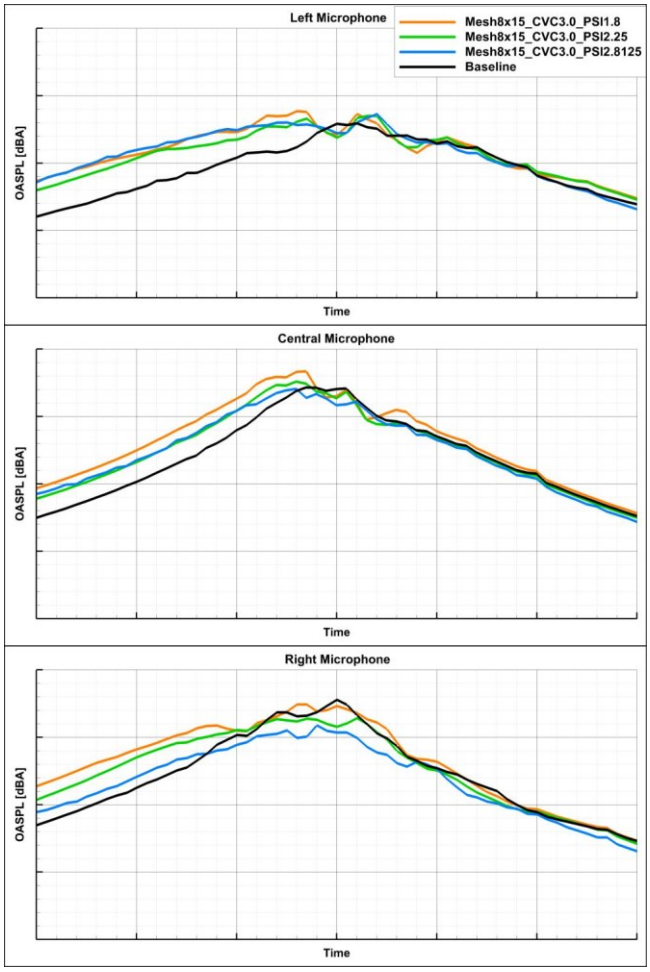

Figure 16 - OASPL along the path for different Δψ and the 8x15 mesh and CVC=3.0 wake refinement

5.3 Isolated MR Unsteady Analysis

Having chosen the best compromise between accuracy and speed, we now move on to analyse an unsteady MR manoeuvre that was optimized for low noise approach. This low noise manoeuvre was obtained using the method developed by Cruz *et al*[6] where a quasi-steady path analysis, based on numerically calculated hemispheres, is used to calculate the on-ground footprint. The optimizer will then continuously adjust the path in order to minimize the on-ground noise footprint. Since this quasi-steady analysis is based on steady manoeuvres, observing that the variations along the path are smooth and no significant accelerations exist, it was decided to interpolate the steady trim data in order to obtain the unsteady trim data to use in EMAA and FAST as shown in Figure 17. The total manoeuvre time is 23.4s and for simplicity the time below is normalized using this value. The aerodynamic solution total calculation time (wall-clock) was 750s on 4 GPU cores, meaning it was 32 times slower than real time. To achieve this calculation speed it was also necessary to limit the free-wake calculations to 3 rotor revolutions. Using only 2 revolutions would result in an unrealistic increase of the rotor Thrust Coefficient (C_T) towards the end of the manoeuvre as the speed decreases and the wake stays closer to the rotor. As shown in Figure 18, with 3 rotor revolutions, the C_T is almost constant throughout the manoeuvre, slightly increasing when the helicopter is decelerating but apparently unaffected by the wake cut-off.

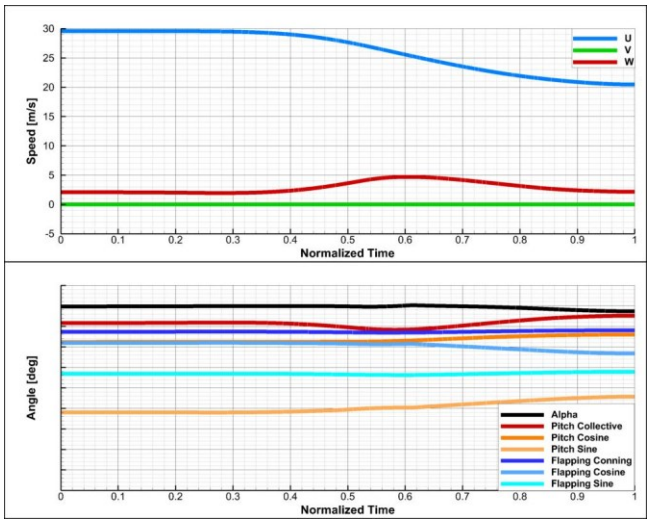

Figure 17 - Unsteady manoeuvre trim data

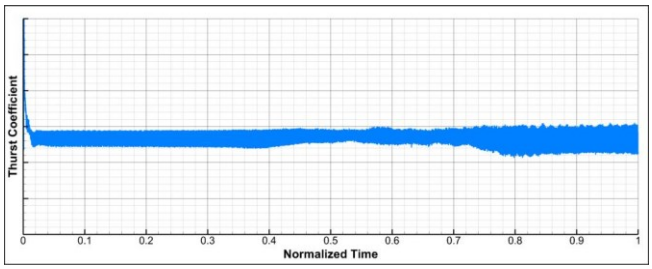

Figure 18 - Unsteady manoeuvre Thrust Coefficient time-history

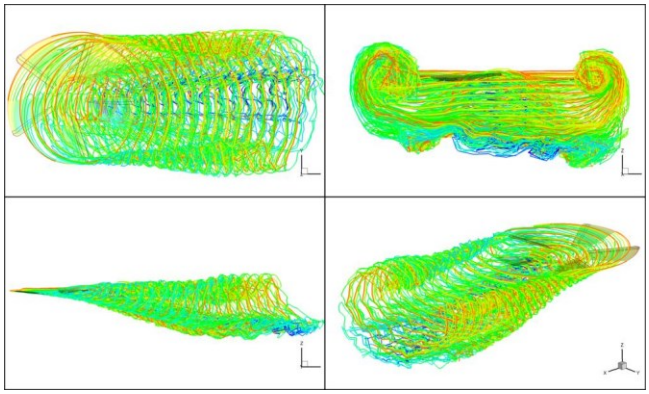

Figure 19 - Wake geometry at a normalized time of 0.20

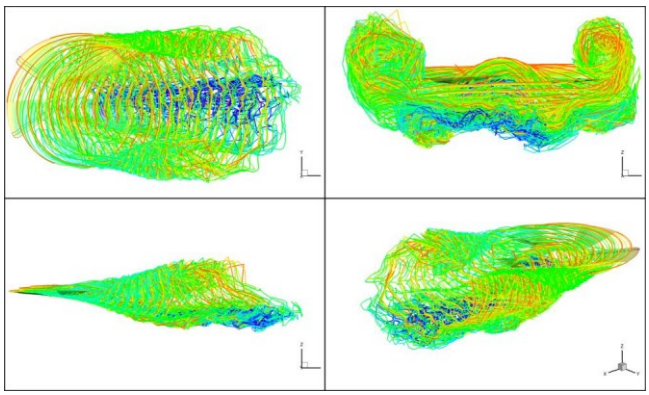

Figure 20 - Wake geometry at a normalized time of 0.65

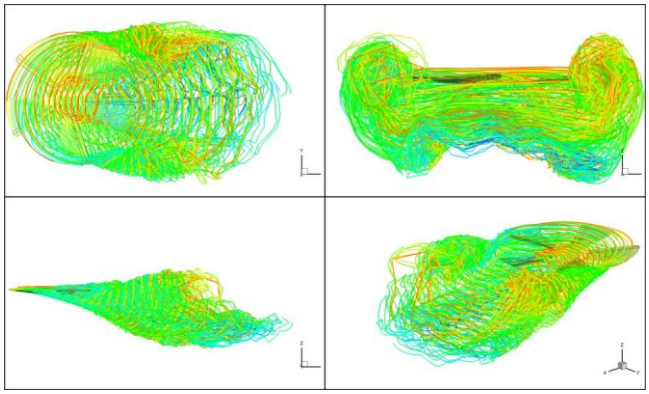

Figure 21 - Wake geometry at a normalized time of 1.00

Since the MR unsteady manoeuvre is part of an optimization study aimed at decreasing the on-ground noise levels, a simple comparison will be made with the steady descent based on the certification Approach condition mentioned earlier. This steady manoeuvre uses the same trim mentioned in §5.2 and detailed in Melone *et al*[22]. The wake refinement and mesh used are the same as the ones used in the unsteady analysis and only 3 rotor revolutions were analysed requiring just 12s to calculate on 4 GPU cores. Note that the Optimized path has the start and finish points made to coincide with the Certification path.

Since the Certification manoeuvre is flown much faster, it was necessary to extend the Optimized manoeuvre acoustic analysis in FAST. This is done by assuming that a steady state has been reached at the end of the Optimized manoeuvre and the aerodynamic loading of the last revolution is repeatedly used until the final acoustic analysis time is reached. The total simulated time was then 40s and it took 22s to calculate the noise on the 3 microphones using only 1 CPU core, almost 2 times faster than real time.

The OASPL-dBA comparison (Figure 23) shows that the Optimized manoeuvre perceived noise is predicted to be lower, especially on the left and central microphones. This although that when the helicopter is approaching the microphones the predicted Sound Pressure (Figure 24) is higher compared to the Certification manoeuvre. This happens because the Optimized manoeuvre is flown at slower speeds and the resulting OASPL-dBA is smaller. The Sound Pressure after the helicopter has passed above the microphones is slightly reduced as are the peak values on all microphones.

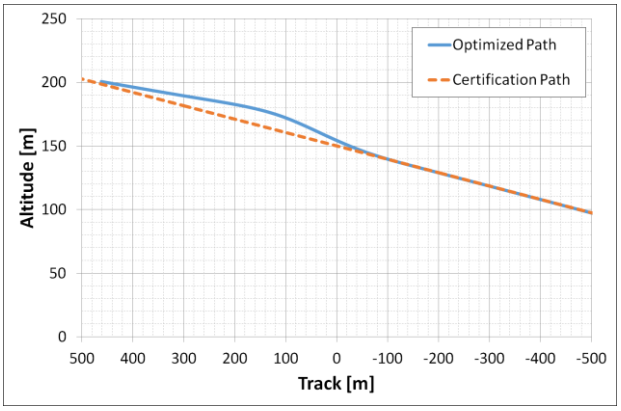

Figure 22 - Optimized path versus Certification path trajectory

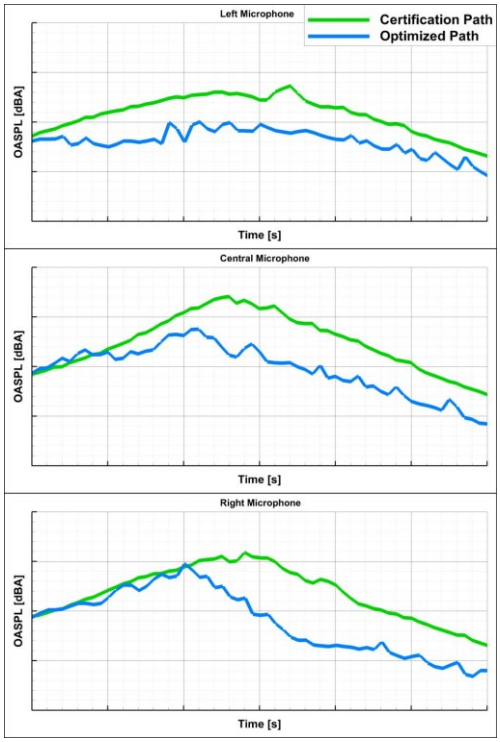

Figure 23 - Comparison between the Certification and Optimized path OASPL-dBA time-history on the 3 certification microphones for the isolated MR case

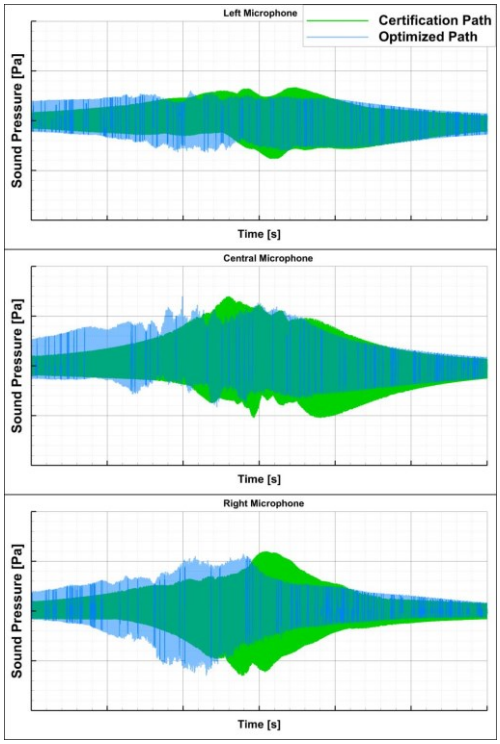

Figure 24 - Comparison between the Certification and Optimized path Sound Pressure time-history on the 3 certification microphones for the isolated MR case

5.4 Coupled MR and TR Unsteady Analysis

The final analysis will focus on a coupled MR and TR unsteady analysis and comparison to the steady Certification manoeuvre. The unsteady aerodynamic and acoustic analysis now include the TR and the trim data is based on the low noise Optimized manoeuvre mentioned in §5.3. The aerodynamic analysis total simulated time was again 23.4s but now the time-step was decreased so that the TR Δψ was 4.0° resulting in a MR Δψ of 0.8°. The TR centre is located 8.4 meters behind and 0.5m to the starboard side (right) relative to the MR centre. The wake cut-off was set at 5 revolutions for both rotors resulting in an aerodynamic solution total calculation time (wall-clock) of approximately 38500s on 4 GPU cores. This increase in calculation time compared to the isolated MR case is explained by the increased number of blades, the 3.5x smaller time-step (MR Δψ of 0.8° instead of 2.8125°) requiring more iterations to simulate the same manoeuvre time and the wake cut-off is now at 5 rotor revolutions rather than 3 for the isolated MR. Note that similar multi CPU aerodynamic tools require around 100x more time to calculate the same aerodynamic solution, which would represent months of compute time. For the acoustic analysis the total simulated time was again 40s and it took 100s to calculate the noise on the 3 microphones using only 1 CPU core, or around 2.5 times slower than real time.

The OASLP-dBA time-history of the Optimized path (Figure 25) demonstrates that the TR has a significant effect on the perceived noise levels when the helicopter is approaching the microphones. This is especially true on the left microphone as the cantilever angle of the TR disk makes the propagation of the Loading noise more directed towards the left of the helicopter. The Certification path (also coupled MR and TR) OASLP-dBA time-history is not significantly affected by including the TR since the helicopter is flying considerably faster (compared to the Optimized path) and the vertical tail plane unloads the TR resulting in a lower noise impact. The Optimized path OASLP-dBA peak levels are still lower on all microphones, confirming the validity of the quasi-steady method in calculating low noise manoeuvres.

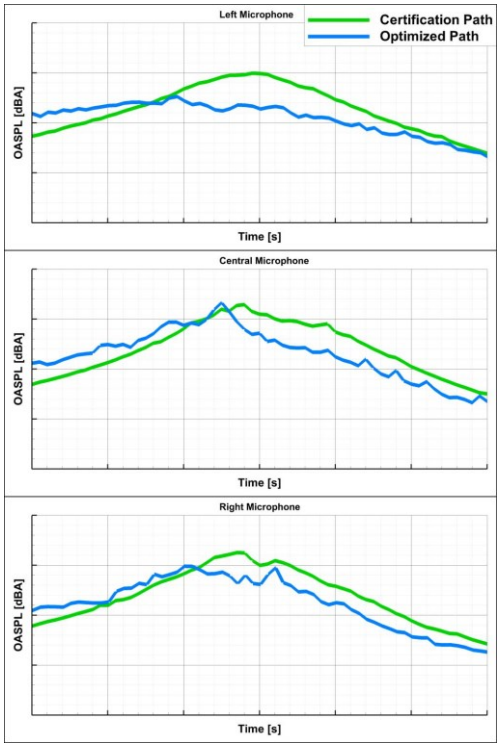

Figure 25 - Comparison between the Certification and Optimized path OASPL-dBA time-history on the 3 certification microphones for the coupled MR and TR case

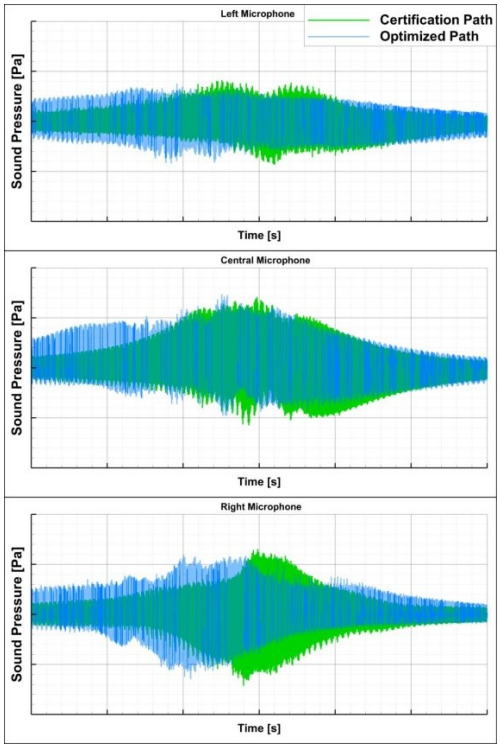

Figure 26 - Comparison between the Certification and Optimized path Sound Pressure time-history on the 3 certification microphones for the coupled MR and TR case

6 Conclusions

This work introduced the development of a new, very efficient aeroacoustic chain inside AgustaWestland, aimed at accelerating the simulation of the noise of helicopter rotors without sacrificing accuracy. The CUDA framework was fundamental to this end, allowing a speedup of more than 1000x on EMAA's free-wake calculations compared to a CPU single core implementation. Even with such a massive speed increase and in order to achieve close to real time simulation, it is still necessary to optimize and carefully reduce the free-wake and blade surface refinement. Still we were able to perform fairly accurate unsteady simulations at only 32 times slower than real time. It should be noted that a simulation of a 4-blade or 3-blade rotor would be closer to real time as the number of wake segments/points would be reduced and the time-step could be bigger. The acoustic tool FAST efficiently implements Farassat's Formulation 1A using the source time dominant algorithm, making its parallelization very efficient. For this work only the CPU version was used because the routines that benefit from the CUDA framework require hundreds of microphones to compensate the overhead of the memory transfers between the CPU and the GPUs.

The unsteady aeroacoustic analysis performed for both the isolated MR and the coupled MR and TR compared an Optimized manoeuvre with the Certification approach manoeuvre on the 3 Certification microphones. The Optimized path was calculated by another aeroacoustic and optimization framework, based on a quasi-steady path analysis, and by comparing with the new aeroacoustic framework we were able to demonstrate the validity of that framework as the noise reduction matched the predictions. Additionally, the introduction of the TR was shown to have a significant effect on the Optimized manoeuvre perceived noise, mostly due to the fact that it was more aerodynamically loaded compared to the Certification path. Further studies should be performed to understand the main source of this perceived noise, if it's mainly TR self BVI or MR and TR interaction induced BVI.

7 Acknowledgements

This research activity is partially funded by the Clean Sky Joint Undertaking under projects GAM-GRC, related to activities performed within the ITD Green Rotorcraft. The authors would like to thank Dr. Sebastian Dubois of the Clean Sky Joint Undertaking for the management monitoring of the program.

8 COPYRIGHT STATEMENT

9 References

[1] H. Ikaida, T. Tsuchiya, H. Ishii, H. Gomi, Y. Okuno, *Numerical Simulation of Real-Time Trajectory Optimization for Helicopter Noise Abatement*, Journal of Mechanical Systems for Transportation and Logistics, Vol. 3, No. 2, 2010

[2] H. Ikaida, T. Tsuchiya, H. Ishii, H. Gomi, Y. Okuno*, Real-Time Trajectory Optimization for Noise Abatement of Helicopter Landings*, Journal of Mechanical Systems for Transportation and Logistics, Vol. 4, No. 2, 2011

[3] K.S. Brentner, L. Lopes, H. Chen, J. F. Horn, *Near Real-Time Simulation of Rotorcraft Acoustics and Flight Dynamics*, , American Helicopter Society 59th Annual Forum, 6-9 May 2003, Phoenix, Arizona

[4] C. C. Hennes, H. Chen, K. S. Brentner, S. Ananthan, J. G. Leishman, *Influence of Transient Flight Maneuvers on Rotor Wake Dynamics and Noise Radiation*, AHS 4th Decennial Specialist's Conference on Aeromechanics, San Francisco, California, January 21–23, 2004

[5] H. Chen, *Rotor Noise in Maneuvering Flight*, PhD Thesis, Pennsylvania State University, December 2006

[6] L. Cruz, A. Massaro, A. D'Andrea, S. Melone, *Rotorcraft Multi-Objective Trajectory Optimization for Low Noise Landing Procedures*, 38th European Rotorcraft Forum, Amsterdam, Netherlands 2012

[7] L. Padula, L. Burley, D. Boyd, A. Marcolini, *Design of Quiet Rotorcraft Approach Trajectories*, NASA/TM-2009-215771, Langley Research Center, Hampton, Virginia, June 2009

[8] A. Le Duc, P. Spiegel, F. Guntzer, M. Lummer, J. Gotz, *Modelling of Helicopter Noise in Arbitrary Maneuvre Flight using Aeroacoustic Database*, Institute of Aerodynamics and Flow Technology, Technical Acoustics Division

[9] M. Syal, J. G. Leishman, Q. Hu, N. A. Gumerov, R. Duraiswami, *Toward Improved Aeromechanics Simulations Using Recent Advancements in Scientific Computing*, AHS 67th Annual Forum, Virginia Beach, May 3–5, 2011

[10] NVIDIA Corporation, *CUDA C Programming Guide*, Version 6.0, July 2014

[11] J. Katz, A. Plotkin, *Low-Speed Aerodynamics*, Second Edition, Cambridge University Press, 2001

[12] J. Gordon Leishman, *Principles of Helicopter Aerodynamics*, Second Edition, Cambridge University Press, 2006

[13] R. L. Bisplingghoff, H. Ashley, R. L. Halfman, *Aeroelasticity,* Addison-Wesley Publishing Company Inc, Boston, 1955

[14] A. D'Andrea, *Development of a Multi-Processor Unstructured Panel Code Coupled with a CVC Free Wake Model for Advanced Analyses of Rotorcrafts and Tiltrotors*, American Helicopter Society 64th Annual Forum, Montréal, Canada, April 29 – May 1, 2008

[15] L. Cruz, *EMAA - Enhanced Multi-GPU Aerodynamic Analysis - Theory and Validation*, AW Internal Report, 2014

[16] F. Farassat, *Derivation of Formulations 1 and 1A of Farassat*, NASA Technical Memorandum *214853, 2007*

[17] G.A. Brès, K. S. Brentner, G. Perez, H.E. Jones, *Maneuvering rotorcraft noise prediction*, Journal of Sound and Vibration 275 (2004) 719–738

[18] K. S. Brentner, C.L. Burley, M.A. Marcolini, *Sensitivity of acoustic prediction to variation of input parameters*, Journal of the American Helicopter Society 39 (3) (1994) 43–52

[19] J. E. Ffowcs Williams, D. L. Hawkings, *Sound Generation by Turbulence and Surfaces in Arbitrary Motion*, Philosophical Transactions of the Royal Society of London. Series A, Mathematical and Physical Sciences, Vol. 264, No. 1151 (May 8, 1969), pp. 321-342

[20] P. A. Di Francescantonio, *New Boundary Integral Formulation for the Prediction of Sound Radiation*, Journal of Sound and Vibration, Volume 202, Issue 4, pp 491-509,15 May 1997

[21] L. Cruz, *FAST - Farassat1A Acoustic Solver Tool - Theory and Validation*, AW Internal Report, 2014

[22] S. Melone, A. D'Andrea, *Helicopter Main Rotor - Tail Rotor Interactional Aerodynamics and Related Effects on the On-Ground Noise Footprint*", 37th European Rotorcraft Forum, September 13th – 15th, 2011, Gallarate, Italy